ANALYSIS OF THE RELATIONSHIPS BETWEEN GEOLOGIC SUBSTRATE AND VEGETATION IN THE WHITE AND INYO MOUNTAINS, EASTERN CALIFORNIA

C. Van de Ven,[*] W. G. Ernst,[*] R. J. P. Lyon,[*] and A. W. Strawa[**1]

1. INTRODUCTION

1.1 Setting and Problem Introduction

The White and Inyo Mountains form the western margin of the Basin and Range Province, being separated from the Sierra Nevada by the Owens Valley (see Figure 1). The central part of the range is underlain by Precambrian and Cambrian metasedimentary strata, primarily quartzites, argillites, and carbonates that strike roughly parallel to the crest of the mountains, and are intruded into by various Mesozoic granitic plutons. Mesozoic andesitic volcanics are present in the northernmost part of this study area. A Basin and Range-style normal fault bounds the western margin of the mountains, resulting in a steep escarpment, rising in about twelve miles from about 4000' above sea level in Owens Valley, to over 14,000' at White Mountain Peak (Hall, 1991). Temperature decreases, with the rise in elevation and precipitation increases, creating numerous microclimatic zones over a short distance. The White and Inyo Mountains are arid, similar to Great Basin desert communities, due to the fact that they are situated within the rain shadow of the Sierra Nevada. At low elevations, desert scrub communities dominate, and a piñon-juniper forest, reminiscent of central Nevada mountains covers the slopes and middle elevations. Vegetation resembles alpine tundra along the crest of the range. As a result of the variety of geologic units and the broad range of topography, the central White-Inyo Range provide excellent opportunities for examining the interrelationships of topography and geology to vegetation.

1.2 AVIRIS Data

To examine vegetation as a function of topography and geology, the spatial distributions of the different variables must first be mapped. Topographic variables can be readily obtained from available USGS digital elevation models (DEMs). To map surficial geology and vegetation, AVIRIS data are used. AVIRIS flightlines were acquired by NASA/JPL over the central White-Inyo Range on September 26 and again, due to cloud cover, on October 7, 1996. Three flightlines of data were obtained. The flightline labeled 01 in Figure 1 (and shown in Figure 8) runs approximately NNW up the crest of the range, following the strike of the sediments, while varying the ground elevation (from low elevation in the south, to higher elevation in the north). This flightline is the focus of this paper. The ground elevation along flightline 01 varies from about 7,500' to over 13,000' above sea level. A second flightline runs perpendicular to the crest of the range, from Owens Valley on the west over White Mountain Peak on the east, and a third extends NW-SE up Waucobi Embayment (flightlines 02 and 03 in Figure 1 respectively). The flightlines cover a nine kilometer swath width, and have a spatial resolution of about 15 by 18 m on the crest of the range.

[1] [*]Dept. of Geological and Environmental Sciences, Stanford University
[**]NASA-Ames Research Center
reply to: vandeven@pangea.stanford.edu

Figure 1. TM image of the White Mountains and surrounding regions. The Sierra Nevada lie just to the west (left) of the scene. The three AVIRIS flightlines are marked. Line 01, along the crest of the range, constitutes the main focus of this paper

2. DATA AND ANALYSIS

2.1 Field Sites

The areal distributions and nature of the bedrock, soil, and botanical cover were assessed through detailed on-the-ground measurements. A total of fifty-eight 50 x 50 m sites (each divided into four quadrants) along the three AVIRIS flightlines were occupied during July, 1997, 1998, and 1999. The sites were selected to cover the range of elevations for each rock type. 44 sites were established in 1997, 34 reoccupied and 13 new sites established in 1998, and, in 1999, 52 sites were reoccupied, and one new site was established. Four to eight investigators estimated the total ground cover for all vegetation species covering at least 1 percent of the area, as well as the total ground cover of each rock type and soil for all four quadrants at each site. The results for all four quadrants were averaged together to give a percent cover across the entire site for all vegetation species, rock types, and soil. Barring catastrophic blowdown, the areal coverage of individual tree species (Mountain Mahogany, Piñon Pine, Juniper, Limber Pine, and Bristlecone Pine) should be nearly invariant over the three-year period of investigation; hence, departures measure the reproducibility of our field techniques. For 1997 forested sites reoccupied in 1998 and 1999, apparent mean differences in areal proportions of tree species range from 0.0 to 3.2 percent, and average 1.1 percent of total vegetation. These differences are acceptably small, and reflect a combination of operator subjectivity and difficulty in reoccupation of the exact sites. The primary field analyses were completed during July of each year, when leaves and flowers were well developed, to aid in vegetation identification. Most of the field sites were reoccupied during late September 1998 and 1999 to assess the vegetation during a similar season as the AVIRIS data (October 7).

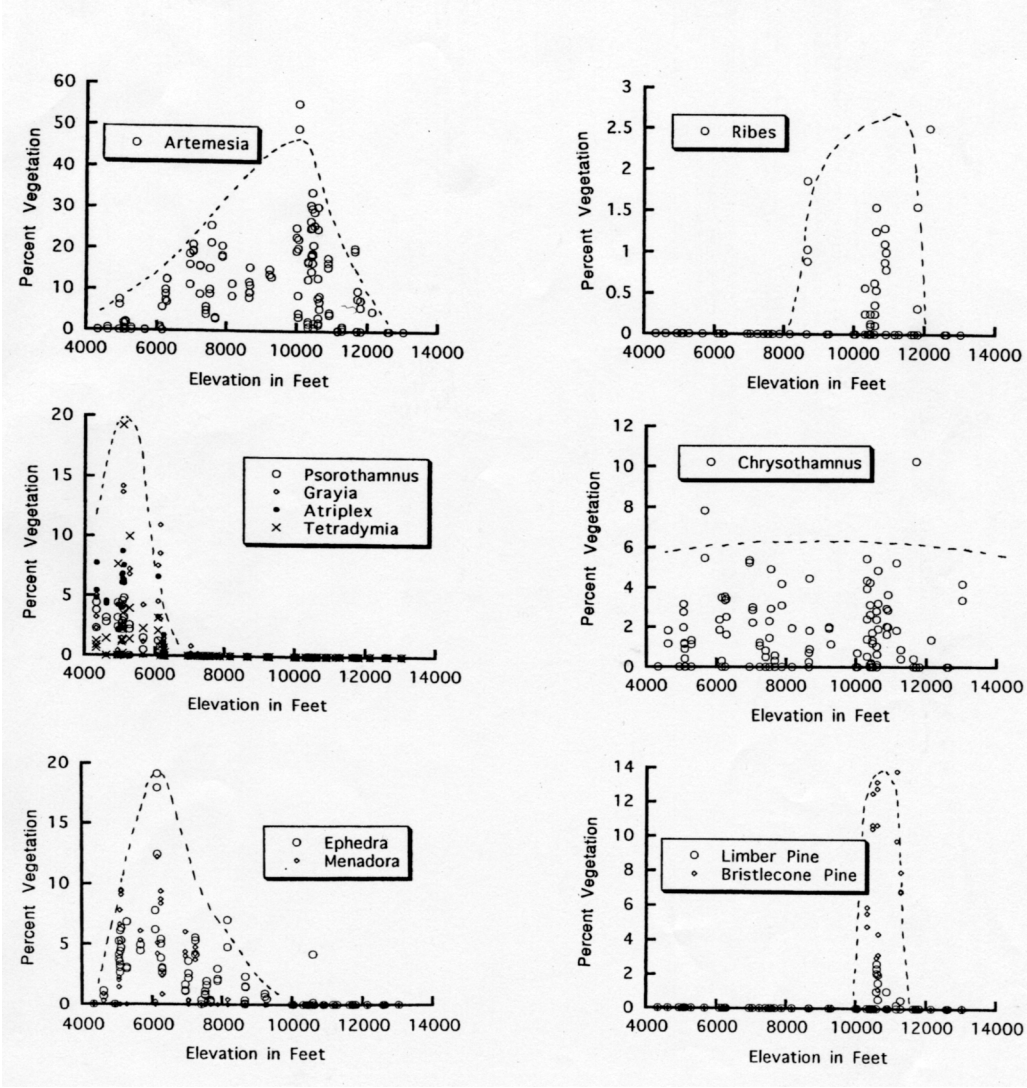

Figure 2. Areal coverage of plants and plant groups as functions of elevation (all bedrock types, July measurements, 1997, 1998, and 1999).

Figure 2 illustrates a small portion of our quantitative botanical data. In the studied mountainous areas, *Grayia*, *Psorothamnus*, *Atriplex*, and *Tetradymia* flourish only below ~6,500,' and individually account for several to 10-15 percent of the total area. *Menadora* is abundant below ~8,000', and *Ephedra* below ~9,000'; each of these species averages approximately 5 percent of the area. In contrast, *Ribes* ranges from ~9,000-12,000', and only makes up about 1 percent of the coverage. *Artemisia* and *Chrysothamnus* are broadly stable throughout the central White-Inyo Range, the former as a substantial component (15 ± 5 percent) of the ground cover, the latter as a minor plant species (about 2 percent of the area). Bristlecone ± Limber Pine frequent slopes of granitoid and carbonate rocks at altitudes of 10,000-11,500'. Total vegetation increases from about 4,000' to 10,000', and declines abruptly at elevations above 11,500'. Our work supports and adds quantitative bedrock, soil, and elevation constraints to earlier, comprehensive syntheses by Mooney (1973) and Morefield (1988).

2.2 Sample Spectra

During July and September field studies in 1998 and again in July, 1999, visible and near infrared spectra were collected using a portable 8-channel (DELPHI) radiometer, operating over the range of 474-950 nm with 25 nm bandpass filters. Nine thousand sets of spectra were collected each of two years, at

least 145 spectra at each 50 x 50 m site (60 vegetation, 60 rock/soil, and 25 white standards). NDVIs (normalized differenced vegetation indices) were calculated for both vegetation and rock/soil, means, and standard deviations were determined for each of the four quadrants. In addition, a mean NDVI (SiteNDVI) was calculated for each site. Although the spectral resolution of the DELPHI radiometer is coarse relative to AVIRIS, it allows examination of field NDVI values, a measure of the relative vitality of the vegetation versus elevation, time (see Figure 3 for both of these), and rock types (not shown in Figure 3).

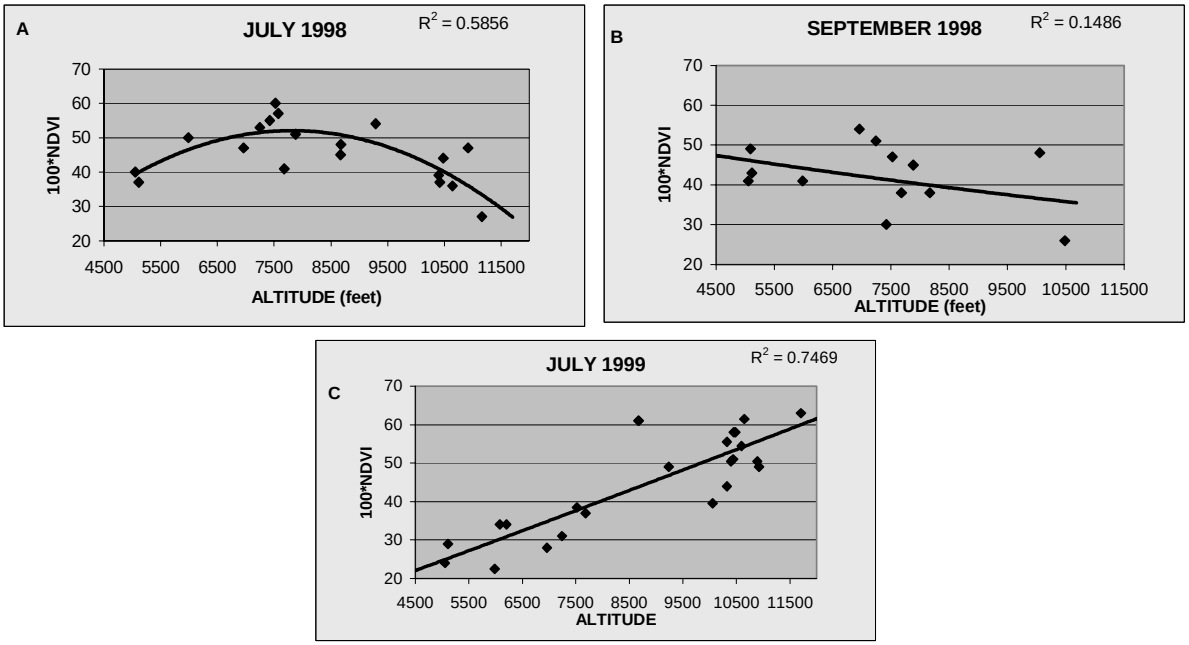

Figure 3 Graphs of average NDVI at field sites from (A) July, 1998 showing an NDVI maximum at middle elevations, (B) September, 1998, showing NDVI apparently independent of elevation, and (C) showing NDVI increasing with elevation.

Graphs of mean NDVI for sites (SiteNDVI) versus altitude for July, 1998 exhibit an arcuate spread, whereas those for September, 1998 display nearly constant NDVI with elevation as shown in Figures 3a, and 3b, respectively. The July, 1999 data show rapidly increasing NDVI with elevation in Figure 3c. Figure 3a is a plot of the July 1998 "SiteNDVI" calculations for field sites versus elevation. The data approximate an arcuate convex shape, which, interestingly, is the same general shape as that for the total vegetation versus elevation, for July, 1997 and 1998. We interpret this pattern as showing a vegetation maximum at the middle elevations in 1998, and the effects of the late winter (El Niño) snowpack inhibiting early summer vegetation growth at higher altitudes. In Figure 3b, the September, 1998 "SiteNDVI's" versus elevation gives a strikingly different plot. In this case, the "SiteNDVI's" decrease with increasing elevation. In July, 1998 the vegetation was at a maximum at middle elevations, and the high-elevation vegetation was just emerging from the late winter snowpack, whereas at low elevations, the vegetation had already reached its peak, dried out, and senesced. The September, 1998 data shows the low elevation sites at about the same NDVIs as in July, as expected near the end of summer. By September, the middle elevation vegetation senesced after their peak in July, and the high elevations peaked sometime between July and September, and are in the process of drying out and dying back. Figure 3c from July, 1999 (La Niña) shows a more typical year, with the vegetation showing maximum vigor at high elevations in July, when the ground is still saturated from the recent snow melt, the middle elevations are nearly dry so the vegetation is beginning to senesce, and the low elevations are already dead.

In addition to the DELPHI spectra, spectrally detailed short-wavelength infrared (SWIR) spectra were collected on rocks and soils using a PIMA spectrometer. It has ~2 nm spectral resolution in the SWIR, 1300-2500 nm. The PIMA spectra provide more direct comparisons with AVIRIS spectra, providing geologic data at locations where the AVIRIS spectra are overwhelmed by the vegetation signal, yield rapid mineralogical information in the field or lab, and provide ground truth for calibration between

field and remotely sensed data. As shown in Figure 4, the PIMA spectra generally match well with USGS library and AVIRIS spectra. Examples of PIMA and mean AVIRIS SWIR spectra for geologic materials are shown in Figure 4 for epidote, dolomite, and calcite. Muscovite spectra are shown in Figure 5. In muscovites, cations, particularly Fe, substitute for octahedral Al, the 2200 nm Al-OH absorption shifts to longer wavelengths, as shown in Figure 5 (Duke, 1994). The Al-OH feature shifts continuously from about 2198 to 2215 nm as the amount of octahedrally coordinated Al decreases. This continuum can be divided into three different spectra with the ~10 nm AVIRIS data, but has been separated into at least five distinct spectra collected by the PIMA. Although it has not yet been confirmed in the central White-Inyo Mountains, it is likely that metamorphic grade increases as the Al-OH feature shifts to shorter wavelengths, from 2215 nm to 2200 nm (Duke, 1994).

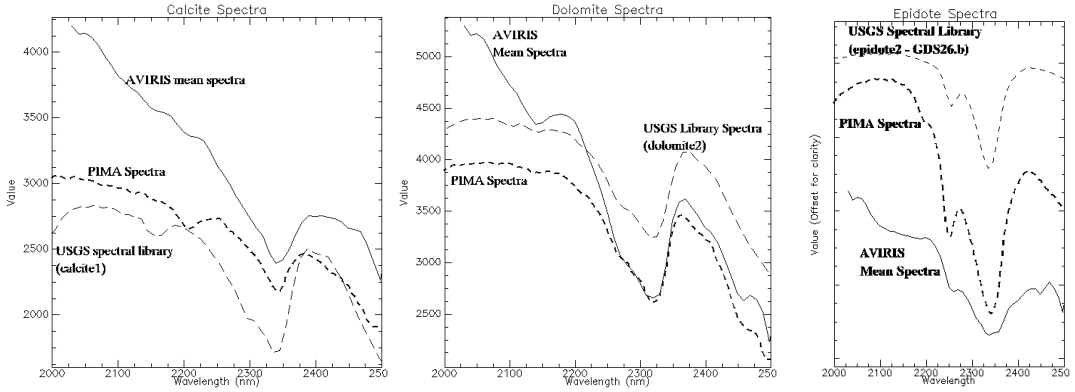

Figure 4. Comparisons of PIMA, mean AVIRIS spectra, and USGS library spectra for calcite (left), dolomite (middle), and epidote (right). The carbonate feature is located at ~2335 nm in calcite and ~2320 nm for dolomite. Epidote has a deep feature at ~2335 nm, as well as a smaller absorption at ~2255 nm. The names of the USGS library spectra are labelled in parentheses.

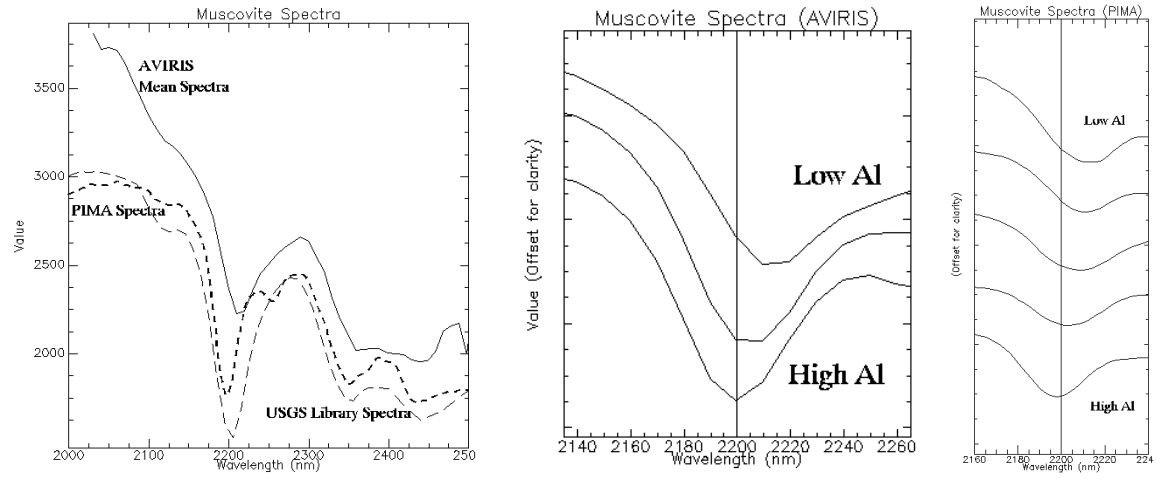

Figure 5. Left: Comparisons of USGS library, PIMA, and mean AVIRIS spectra. Middle: Shifts of the Al-OH absorption feature in muscovites (and sericites) from AVIRIS spectra – (top spectra is the mean of the orange class in Figure 7c, middle= yellow class, and bottom= brown class). Right: PIMA spectra of the Al-OH shift. Due to the better spectral resolution of the PIMA spectra (about 2nm) compared to the AVIRIS spectra (about 10 nm), smaller differences in the wavelengths of this feature can be detected.

2.3 AVIRIS Analysis

Analyses of AVIRIS data were accomplished using ENVI 3.2, following the "hourglass" strategy described in ENVI tutorials and users manuals (RSI, 1999), and will be described only briefly here. The goal of this approach is, through a process of reducing the amount of data being examined, to (1) locate the spectral endmembers that can be combined linearly to explain the spectra throughout the scene, (2) identify the compositions of the endmembers, and (3) map the proportions of each endmember in every pixel throughout the AVIRIS scene. Our AVIRIS data were converted to reflectance at JPL using the method described by Green et al. (1993); residual noise was reduced using the EFFORT smoothing algorithm (Boardman, 1995). An MNF (Minimum Noise Fraction) transform is run on the reflectance data, which is a pair of cascaded principal components analyses creating a new data set from the original, concentrating the noise in the higher numbered bands. The purpose of this transform is to segregate the noise from the data by ranking the MNF output files by signal-to-noise ratio (SNR). Further analyses are performed only on the bands containing data (high SNR). After the MNF, a Pixel Purity Index (PPI), is run. The PPI score is computed by repeatedly projecting n-dimensional scatterplots of the MNF data onto a random unit vector. The outlier pixels in each projection are recorded and the number of times each pixel is marked as extreme is its PPI score. The higher the PPI score, the more likely a given pixel is a spectral endmember. All pixels with a user-defined high PPI score are then projected into n-dimensions (n is the number of MNF bands being examined). Assuming linear mixing, the endmember pixels are outliers from the cloud of data, and the spectral mixtures are located between the endmembers in spectral space. After the identification of spectral endmembers, their distributions were mapped across the AVIRIS scene using the Mixture Tuned Matched Filtering (MTMF) classification algorithm. The resulting output yields a separate MTMF score for each endmember at each pixel, with scores ranging from 1.0 (signifying 100% of a pixel is composed of that endmember) to 0.0 (signifying none of that endmember is found in that pixel). An infeasibility scene for each endmember is also output from the MTMF classification. The infeasibility score for each pixel gives a measure of how likely the pixel's classification is a "false positive," or, in other words, was given an erroneously high MTMF score. The infeasibility scenes allow some control over the accuracy of the results by identifying misclassified pixels.

It was difficult to locate all of the vegetation endmembers through n-dimensional analysis, inasmuch as the dry vegetation generally did not plot as distant outliers. Upon examination of the visible and near-infrared AVIRIS bands (about 400-1350 nm), several healthy, green vegetation endmembers were identified through this method. Spatially, this vegetation was found around springs and along streams in valley bottoms, but not in the broad meadows along the range crest, which comprises the majority of flightline 01 (see Figure 7a). The AVIRIS data were obtained in early October, when most vegetation senesced, particularly the sagebrush and grassy alpine meadows. This dry vegetation has low NDVIs and relatively flat spectra. Figure 6 presents examples of green and dry vegetation examples. There is little to distinguish the dry vegetation spectra, and therefore it receives low PPI scores. Thus, pixels with low PPI scores need to be included in the n-dimensional visualizer, increasing the number of pixels examined, and thus making it easier for those pixels to be lost in the data cloud. One strategy to locate these endmembers in spectral space might be to spatially subset the data rather than examine the entire flightline at once. By examining smaller areas, and therefore fewer pixels, more subtle endmembers might become apparent. Another strategy would be to incorporate DEM (topographic) data in the analysis, taking advantage of the fact that vegetation is often strongly dependent on elevation. However, these strategies have yet to be attempted for these data.

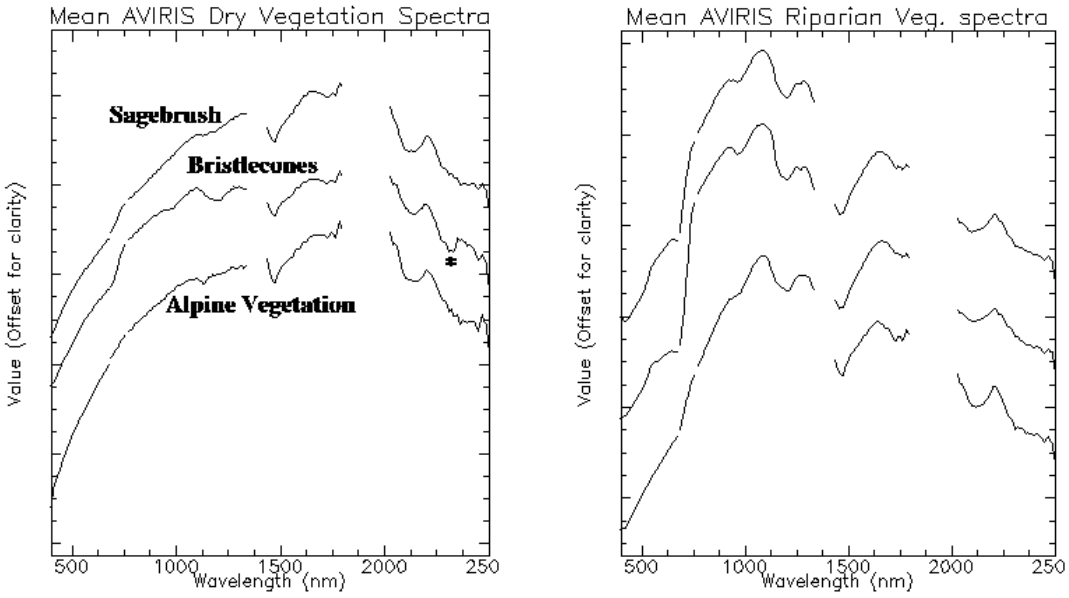

Figure 6. Comparisons of mean AVIRIS spectra of dry vegetation classes (left) and "green" riparian vegetation classes (right). Note the steep slope in reflectance from about 700 nm to 1000nm (the red edge) in the riparian vegetation. An example of spectral mixing is evident in the Bristlecone spectrum, which has an overall vegetation pattern, but contains a carbonate feature at ~2320 nm (denoted by *) due to the fact that these trees typically grow widely spaced over dolomite rocks and soils, allowing underlying bedrock and soil spectrum to be detected.

To map the distributions of the dry vegetation, “endmembers” were selected from pixels whose vegetation was known from quantitative fieldwork. Pixels whose vegetation is composed of sagebrush meadow, alpine meadow, and Bristlecone pine communities were simply selected, and their distributions mapped using the MTMF. The results of that mapping are given in Figure 7b.

3. RESULTS

The iron-bearing minerals, micas, and carbonates of the surficial geology were mapped employing 1996 AVIRIS data (see Figure 7c). The primary successes of the mineralogic mapping have been with the volcanic and carbonate units. The results of these analyses show good correlation between published geologic maps and mineral distributions, whereas other units, notably vegetation-covered granitoids, and some of the quartzites and argillites have not been clearly differentiated (Ernst, et al., 1993). The Reed Dolomite has been distinguished from limestone units found within the Wyman, Deep Spring, and Poleta Formations based on the location of the carbonate absorption. The carbonate feature in calcite is found at 2348nm, while the same feature for dolomite is located at shorter wavelengths, namely 2319 nm (see Figures 4 and 7c).

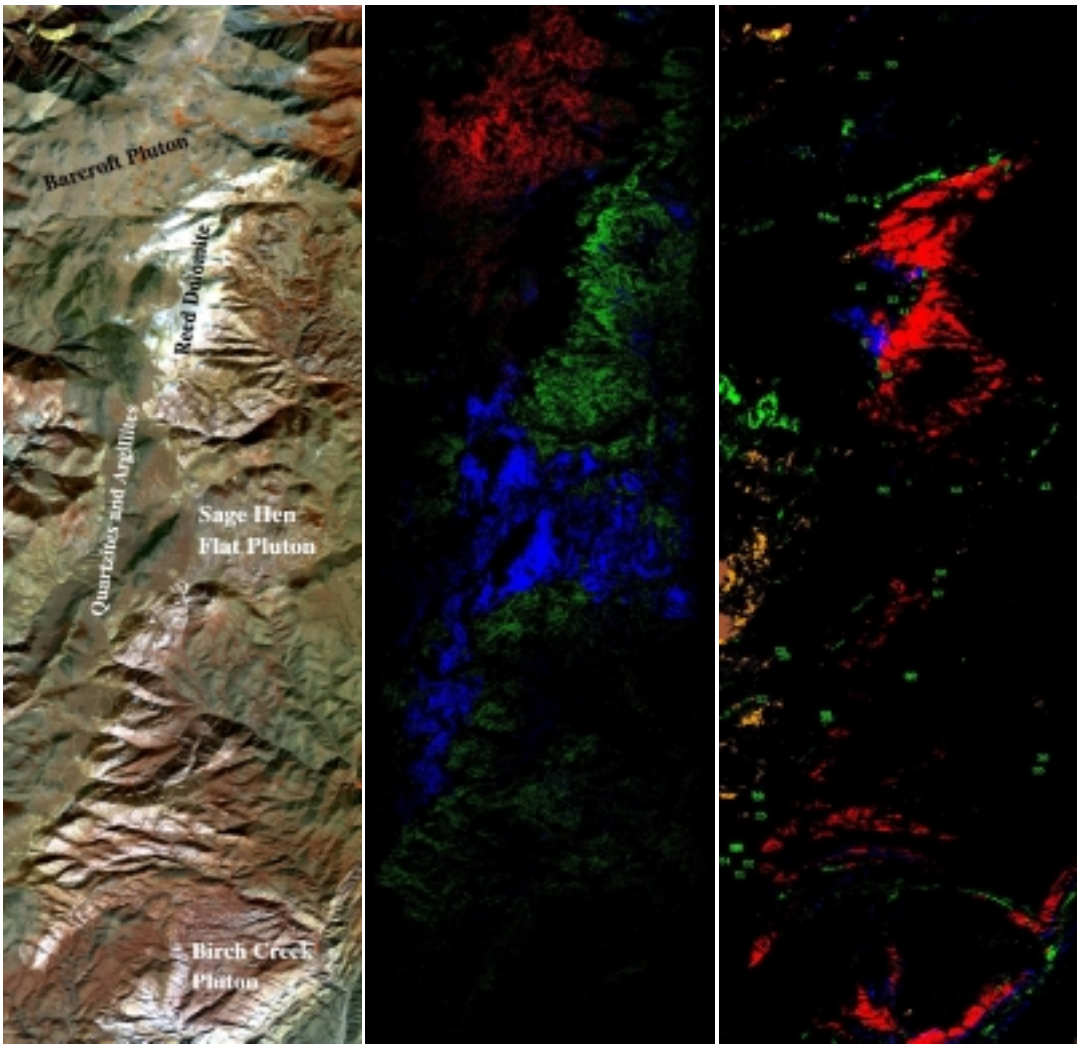

A **B** **C**

Figure 7.
A: Color infrared image of central White Mountains (Red=840 nm, Green=645nm, and Blue=460nm). The major plutons and metasedimentary rocks are labeled (from Ernst et al., 1993).
B: MTMF output of three dry vegetation classes representing the following vegetation communities: R= alpine meadows, G = Bristlecone pines, and B= sagebrush meadows, where brightness is proportional to percent of cover for a given community.
C: MTMF result of geologic classes representing: R= dolomite, G= epidote, and B= calcite (where brightness is proportional to percent cover) overlain by muscovite classes (shown as regions of interest from ENVI) colored orange, yellow, and brown in the upper left corner, and along the left side of the image. For mean spectra of the muscovite classes, see Figure 5. Field sites are numbered in green.

Intraformational changes have also been mapped. Variations in the metavolcanics north of the Barcroft pluton can also be mapped based on the shifts in the Al-OH absorption associated with sericite (fine-grained muscovite). The Al-OH feature mapped from the AVIRIS data varies from 2200 to 2220 nm within metavolcanic units (see Figure 4), indicating variability of Al content within a mapped formation, and may represent a metamorphic gradient. An epidote lens has been identified along the southern contact of the Barcroft pluton near the Reed Dolomite. In the southern end of flightline 01, around the Birch Creek pluton, a metamorphic aureole is evident in the surrounding carbonate and pelitic layers. When the entire flightline was unmixed as a whole (Figure 7), metasediments around the pluton mapped as simply dolomite and calcite. However, when just the the pluton and surrounding units were analyzed, additional spectral

classes became evident, including garnet (hydrogrossular) and dolomite + tremolite (see Figure 8). A spectral class mapped as dolomite is found between the garnet and dolomite + tremolite zones, but other metamorphic minerals, particularly wollastonite most likely coexist in these rocks. However due to the weak spectrum of wollastonite, it was not identified spectrally.

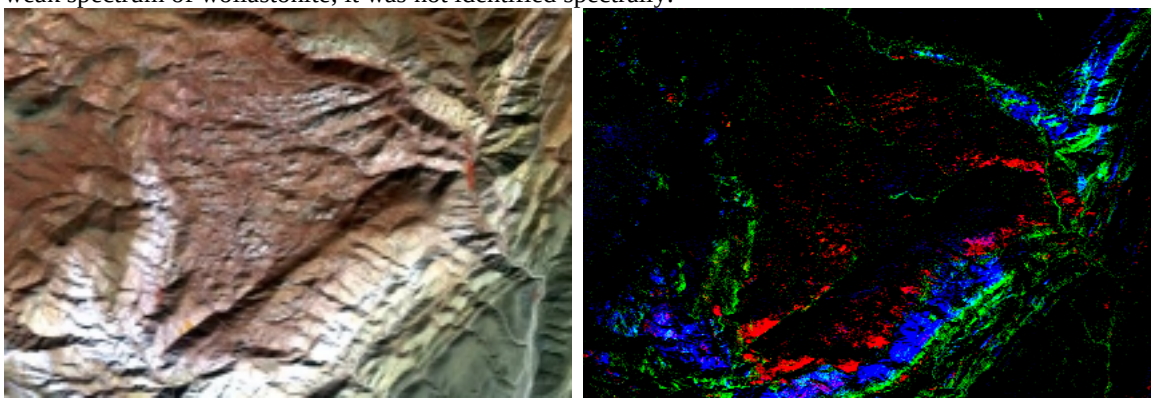

Figure 8. Left: Color infrared image of the Birch Creek pluton and surrounding area (R=839nm, G=646 nm, and B=458 nm). Right: MTMF result, where R=hydrogrossular, G=dolomite + tremolite, and B=dolomite. The brightness of each pixel is proportional to percent cover. Mixtures of these three classes are shown as cyan (B+G), magenta (R+B), and yellow (R+G).

Based primarily on visible and near infrared spectra, multiple vegetation classes have been mapped. Green vegetation was divided into several classes based on spectral analysis, while dry vegetation endmembers were located based on their spatial relationships and field data. The majority of the vegetation senesced by the time the AVIRIS data were taken. Nearly all of the ground truth consists of vegetation that is dry by autumn (when the AVIRIS data were obtained), such as sagebrush and grasses, leaving most of the green vegetation classes unidentified. In the White Mountains during October, most of the green vegetation is located around permanent springs and streams in valley bottoms. When no reasonable vegetation spectral classes covered the high altitude meadows along the crest of the range, locations where the vegetation was known from fieldwork were selected as endmembers and entered as classes in the mixture-tuned matched filter classification. The results of this MTMF classification are shown in Figure 7b.

As a check on the remote sensing analyses, the basic relationships from remote sensing data can be compared to relationships deduced from field data. We have successfully described and confirmed three important vegetation communities covering much of the central portion of the flightline. In general, field sites within the Barcroft pluton, the highest elevation sites, are dominated by ground-hugging vegetation such as short grasses, small flowers, and cushion buckwheat (*Eriogonum*), which comprise the alpine meadow community. Slightly lower elevation sites, primarily on metaclastic rocks and the Sage Hen Flat pluton, are strongly dominated by sagebrush (*Artemesia tridentata*), with lesser amount of rabbitbrush (*Chrysothamnus sp.*), grasses, and various flowers. This vegetation was grouped into the sagebrush meadow community. A third general community comprises the Bristlecone Pine community, which, besides Bristlecone pines (*Pinus longaeva*), has little other vegetation, although small percentages of grasses, Limber Pines (*Pinus flexilis*), and isolated sagebrush and/or rabbitbrush are common. As anticipated, field sites described using these communities are found within the areas mapped by three distinct, spatially extensive vegetation classes from AVIRIS data. Other less extensive vegetation communities such as that dominated by Mountain Mahogany (*Cercoparpus ledifolius*), for which we have established only two field sites, cover smaller areas, and for that reason, are less likely to correlate with spectral vegetation communities. Identifying the vegetation communities corresponding to the mapped AVIRIS spectral vegetation classes is the primary goal of fieldwork in summer, 2000.

4. CONCLUSIONS

The analysis of the AVIRIS data mapped the carbonate and metavolcanic units closely to published maps. Unfortunately, most of the granitic, quartzite, and argillite rocks were not differentiated based on mineralogic spectra due to nearly uniform vegetative cover. However, that vegetative cover can

be used to approximate the areal extents of some of the underlying geologic substrate. The alpine meadow vegetation community is found in high elevation meadows, corresponding almost exclusively to the area underlain by the Barcroft pluton (see Figure 7a and b). Sagebrush meadows correlate with metaclastic units, such as quartzites and argillites, and the Sage Hen Flat Granite. By examining the vegetation classes, inferences can be made about the relationships between the vegetation and the geologic substrate.

General relationships between vegetation distributions and the underlying rock types were determined as follows: (1) Bristlecone Pines grow in dolomite bodies at high elevations, as well as along the perimeter of the Sage Hen Flat pluton. (2) At high elevations, the Barcroft Granodiorite is almost exclusively covered by an alpine-tundra vegetation community. (3) An association of sagebrush meadows with quartzite, argillite, and the Sage Hen Flat Granite, is evident. These relationships have been confirmed from our field data. Vegetation maps have also been produced along the flightline, although less complete control on the identification of vegetation classes have been made due to a lack of previously published maps.

The observed vegetation ranges are systematic and quantitatively reproducible in the central portion of the White-Inyo Mountains. Particular species and their abundances reflect chiefly the attendant microclimatic conditions, and, to lesser extents, the soil development and the geologic/mineralogic nature of the bedrock. As a consequence, the indexing of AVIRIS hyperspectral data employing *in situ* measurements of plant species and proportions, combined with on-the-ground spectral measurements has allowed initial analyses of relations between vegetation and local conditions.

5. ACKNOWLEDGEMENTS

We are grateful for support by Stanford University (McGee and Shell grants), NASA (Grant NAG5-4888), Texaco (Exploration & Production Dept.), and the University of California White Mountain Research Station.

6. REFERENCES

Boardman, J. W., 1998, "Post-ATREM Polishing of AVIRIS Apparent Reflectance Data Using EFFORT: a Lesson in Accuracy Versus precision," Summaries of the Seventh AVIRIS Workshop, JPL Publication 97-21, Jet Propulsion Laboratory, Pasadena, CA vol. 1, pp. 53.

Duke, E. F., 1994, "Near infrared spectra of muscovite, Tschermak substitution, and metamorphic reaction progress: Implications for remote sensing," Geology, v.22, p.621-624

Ernst, W. G., C. A. Nelson, and C. A. Hall, 1993, Geology and metamorphic mineral assemblages of Precambrian and Cambrian rocks of the central White-Inyo Range, eastern California, 1:62,500, California Division of Mines and Geology, Map Sheet 46, accompanying text 26p.

Green, R. O., J. E. Conel, and D. A. Roberts, 1993, "Estimation of Aerosol Optical Depth and Calculation of Apparent Surface Reflectance (AVIRIS) Using MODTRAN2," SPIE Conf. 1937, Imaging Spectrometry of the Terrestrial Environment, 12p.

Hall, C. A. Jr., ed., 1991, Natural History of the White-Inyo Range, Eastern California, Univ. of California Natural History Guides, v. 53, pp. ix-xi.

Mooney, H. A., 1973, "Plant communities and vegetation," in R. M. Lloyd, and R. S. Mitchell (eds.), A Flora of the White Mountains, California and Nevada, University of California, Berkeley, p. 7-17

Morefield, J. D., 1988, "Floristic habitats of the White Mountains, California and Nevada: A local approach to plant communities," in C. A. Hall, Jr., and V. Doyle-Jones (eds.), Plant Biology of the Eastern California, White Mountain Research Station Symposium, v. 2, p. 1-18.

RSI, 1999, ENVI Tutorials, The Environment for Visualizing Images, version 3.2, Research Systems, Inc., Boulder, CO, USA.